



HAL
open science

Cation exchanged Fe(II) and Sr compared to other divalent cations (Ca, Mg) in the Bure Callovian-Oxfordian formation. Implications for porewater composition modelling.

Christophe Tournassat, Catherine Lerouge, Philippe Blanc, Jocelyne Brendle, Jean-Marc Greneche, Stéphane Touzelet, Eric C. Gaucher

► **To cite this version:**

Christophe Tournassat, Catherine Lerouge, Philippe Blanc, Jocelyne Brendle, Jean-Marc Greneche, et al.. Cation exchanged Fe(II) and Sr compared to other divalent cations (Ca, Mg) in the Bure Callovian-Oxfordian formation. Implications for porewater composition modelling.. Applied Geochemistry, 2008, 23 (4), pp.641-654. 10.1016/j.apgeochem.2007.11.002 . hal-00597171

HAL Id: hal-00597171

<https://brgm.hal.science/hal-00597171v1>

Submitted on 31 May 2011

HAL is a multi-disciplinary open access archive for the deposit and dissemination of scientific research documents, whether they are published or not. The documents may come from teaching and research institutions in France or abroad, or from public or private research centers.

L'archive ouverte pluridisciplinaire **HAL**, est destinée au dépôt et à la diffusion de documents scientifiques de niveau recherche, publiés ou non, émanant des établissements d'enseignement et de recherche français ou étrangers, des laboratoires publics ou privés.

Cation exchanged Fe(II) and Sr compared to other divalent cations (Ca, Mg) in the Bure Callovian-Oxfordian formation. Implications for porewater composition modelling.

Christophe Tournassat^{a*}, Catherine Lerouge^a, Philippe Blanc^a, Jocelyne Brendlé^b, Jean-Marc Greneche^b, Stéphane Touzelet^a and Eric C. Gaucher^a

^a BRGM, F 45060 Orléans, France

^b LMPC, ENSC, F 68093 Mulhouse, France.

^c LPEC, Université du Maine, F 72085 Le Mans, France

*Corresponding author and mailing address:

Christophe Tournassat

BRGM

Environment and Process Division (EPI/MIS)

3 Avenue Claude Guillemin

45060 Orléans Cedex 2, France

E-mail: c.tournassat@brgm.fr

Tel: +33 (0)2 38 64 47 44

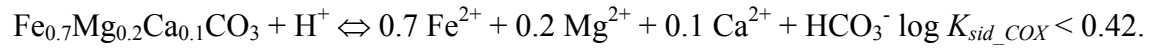
Fax: +33 (0)2 38 64 30 62

Abstract

Fe and Sr bearing phases were thoroughly investigated by means of spectrometric and microscopic techniques in Callovian-Oxfordian (COX) samples originating from the ANDRA Underground Research Laboratory (URL) in Bure (France). Sr was found to be essentially associated with celestite, whereas Fe was found to be distributed over a wide range of mineral phases. Fe was mainly in its +II oxidation state in the studied samples (~93 % from Mössbauer results). Most of the Fe(II) was found to be present in pyrite, sideroplesite/ankerite and clay minerals. Iron +III, if present, was associated with clay minerals (probably illite, illite-smectite mixed layer minerals and chlorite). No Fe(III) oxi(hydro)xide could be detected in the samples. Strontianite was not observed either. Based on these observations, it is likely that the COX porewater is in equilibrium with the following carbonate minerals, calcite, dolomite and ankerite/sideroplesite, but not with strontianite. It is then shown that this equilibrium information can be combined with clay cation exchange composition information in order to give direct estimates or constraints on the solubility products of these carbonate minerals: dolomite, siderite and strontianite. As a consequence, an experimental method was developed to retrieve the cation exchanged Fe(II) in very well preserved COX samples.

The very homogeneous cation exchange composition of the formation is completely in agreement with a homogeneous presence of calcite and dolomite minerals whose equilibrium reactions control part of the porewater composition. Amongst the broad range of values available for dolomite solubility products in thermodynamic databases, the value of $\log K_{dolomite} = -3.57$ is the most appropriate for the one present in the COX formation. As regards strontianite, it appears that the equilibrium constant tabulated in the Llnl database is not valid for natural clay systems. The value given in Busenberg et al. *Geochimica et Cosmochimica Acta*, 48, 2021-2035, used by most of the other available thermodynamic

databases seems to be far more appropriate. Concerning Fe(II) and siderite/ankerite equilibrium, the measured Fe/Ca ratio on the clay exchanger (~0.01) could only be considered as a maximum value due to possible experimental bias, leading to the following constraint for the solubility of the sideroplesite phase present in the COX:



This constraint is in agreement with the estimated solubility of this phase based on a solid solution model: $\log K_{sid_COX} = 0.23$.

Keywords: dolomite, strontianite, siderite, cation exchange, Callovian-Oxfordian, porewater composition.

1. Introduction

The French National Radioactive Waste Management Agency (ANDRA) is building an underground research laboratory (URL) in Bure (north eastern France) in order to study the disposal of radioactive waste in a deep clay formation. The main gallery is located in a Callovian–Oxfordian formation (COX) at an approximate depth of 490 m. To assess the durability of materials (glass, stainless steel, concrete, engineered clay barrier, etc.) and determine the speciation and related mobility of the radionuclides in the host rock formation, it is necessary to define the chemistry of the COX porewater. A modelling work program has been dedicated to this topic for several years, based on thorough investigations of the mineralogical composition and physical properties of the COX formation (Gaucher et al., 2004) and has led to a first estimate of the COX clay rock porewater composition (Gaucher et al., 2006).

This porewater composition model still has some deficiencies that need to be solved. Amongst them, the control of iron solute concentration and subsequent redox control in the formation needs to be improved in order to better simulate redox perturbation in the COX (redox sensitive radionuclide migration, mineral transformations due to the gallery opening to air atmosphere, nitrate plume coming from class B wastes, etc., see the ANDRA “Dossier 2005” report (ANDRA, 2005) for more details). For instance, the modelled Fe(II) porewater concentration and redox potential modelled by Gaucher et al., 2006, leads to water compositions supersaturated related to Fe(III) oxi(hydr)oxides although none of these Fe(III) phases have been observed on COX samples preserved from oxidation (Gaucher et al., 2004). This inconsistency could be linked to two main hypotheses: (1) a problem of sample observation where Fe(III) oxi(hydr)oxides could have been missed or (2) a problem with the

model. Hypothesis (1) is unlikely, given the repeated observations made on a wide variety of samples by different laboratories and leading to the same conclusion (see data compiled in Michel et al., 2006, the COX database in Access© format is available upon request to the corresponding author of the present paper). Hypothesis (2) could be linked to a misunderstanding of the thermodynamic equilibrium governing the Fe and redox system or a problem originating from the thermodynamic database used for the calculations made in Gaucher et al., 2006. The same type of problem occurs for the Sr concentration in the model that should lead to an oversaturation of strontianite (SrCO_3), although this mineral has not been observed.

As a consequence, the sample preservation (1) and the thermodynamic database (2) hypotheses were tested in the present paper step by step:

(A) Firstly, a thorough examination of iron and strontium bearing mineral phases was performed using various microscopic and spectrometric techniques on very well preserved samples using a liquid N_2 sample preservation and transport procedure (Gehin et al., 2007).

(B) Secondly, it is shown how to use the clay exchanger composition and exchange equilibrium equations to constrain the thermodynamic solubility products of carbonate minerals in clay formations. Thus, an experimental method was developed to retrieve the cation exchanged Fe(II) in very well preserved COX samples in order to add constraints to the Fe(II) carbonate system.

(C) Given the broad range of solubility values available in the literature for strontianite (SrCO_3), dolomite ($(\text{Ca, Mg})(\text{CO}_3)_2$) and siderite (FeCO_3), these theoretical and experimental approaches were combined to select appropriate thermodynamic solubility values for these minerals.

2. Materials and Methods

2.1 Callovian-Oxfordian rock samples

Samples used for the recovery of cation exchanged Fe(II) on clay minerals and Mössbauer analysis were taken directly from the drill-core performed for the PAC (water sampling for chemical and isotope analysis) experiments in the ANDRA URL (Bure, Meuse Haute-Marne, France) in December 2005 (borehole PAC-1002, sample EST 25687). The core was obtained by nitrogen drilling instead of oil-based mud drilling, thus reducing contact with atmospheric O₂. As soon as the core was brought to the surface (~1 h after drilling), a hammer was used to sample rock fragments, which were immediately introduced into a Dewar flask containing liquid N₂ (77 K) to avoid any further oxidation with atmospheric O₂. The samples were then stored in a Dewar flask. The claystone samples used in this study were taken from the centre and the periphery of the core. The liquid N₂ sample preservation towards oxidation has been successfully tested in a former study (Gehin et al., 2007).

Only a small part of the core could be stored in liquid nitrogen Dewar flasks. The remaining parts of the core were placed in Ar and He gas conditioning cells for preservation and further gas analysis (Gaucher et al., 2004; Gaucher et al., 2006; Girard et al., 2005). These samples were used for mineralogical investigations by optical microscopy, SEM, TEM and electron microprobe. For these mineralogical investigations, Callovian-Oxfordian samples originating from other cores (namely samples EST 12436, EST 21400, EST 25380 and EST 20714) were also used.

2.2 Synthetic montmorillonite samples

The synthetic sample is the same as that used in the Gehin et al. Fe(II) adsorption study (Gehin et al., 2007). The synthesis of montmorillonite having the theoretical formula: $\text{Na}_{0.30}[(\text{Al}_{1.7} \text{Mg}_{0.30} \square) \text{Si}_4 \text{O}_{10} (\text{OH}, \text{F})_2] \cdot n \text{H}_2\text{O}$ was performed in acidic and fluoride medium under hydrothermal conditions (Reinholdt et al., 2001). A hydrogel having a 1 SiO_2 : 0.212 Al_2O_3 : 0.075 MgO : 0.075 Na_2O : 0.05 HF : 96 H_2O molar composition was prepared starting from water, hydrofluoric acid, sodium and magnesium acetate, silica and aluminium oxide. This mixture was matured for 2 hours at room temperature before being hydrothermally treated in a PTFE lined stainless steel autoclave at 493 K for 72 hours under autogeneous water pressure. After crystallization, the product was separated by filtration and thoroughly washed with distilled water. The pH of the supernatant was 3.5 - 4.5. After drying for one night at 338 K, the sample was placed in a controlled humidity chamber ($P/P_0 = 80\%$, where P represents the saturated vapour pressure over the sample at 298 K and P_0 the saturated aqueous vapour pressure at 298 K). Ca-montmorillonite was obtained by saturation of the prepared Na-montmorillonite with a 0.05 M aqueous solution of CaCl_2 . After treatment, the solid suspension was N_2 -degassed, before being placed in a glove box.

2.3 Extraction of cation exchanged Fe(II) from the Callovian-Oxfordian samples

Two measurement campaigns were carried out: the first was performed on a sample representative of the centre of the core. The second one was performed on a sample localized originally on the periphery of the core. Claystone samples were transferred from the liquid N_2 Dewar directly into the glove box. Claystone samples were then crushed in an agate mortar in a <0.1 and 23 ppm O_2 atmosphere for the central and periphery sample respectively.

The following procedure was entirely performed under a <0.1 ppm O_2 atmosphere. A mass m_{sample} ($\sim 0.3 - 0.5$ g) of sample was precisely weighed on a mg precision balance (Sartorius Basic BA310S) and deposited as a dry powder on a Millipore, Millex-VV, PVDF sterile 0.1 μm filter. 2.5 mL of a solution containing 4.18 mol L^{-1} acetic acid (purity grade $> 99.5\%$), 2.45 mol L^{-1} sodium acetate (purity grade $> 98\%$) and 1.64 mmol L^{-1} 1,10-phenanthroline hydrochloride (purity grade $> 99\%$) were then added to the filter holder at $298 \pm 1\text{K}$. The resulting suspension was immediately filtered under vacuum using a hand-pump. 2.5 mL of the same solution was then immediately added and filtered identically. The resulting filtrate was orange-coloured, in agreement with the absorbance colour of the Fe(II)-phenanthroline complex (Rodier, 1996). The total filtration time did not exceed one minute. The Fe(II) concentration in the filtrate was then measured by absorbance photometry ($\lambda = 510$ nm) using an ATI Unicam spectrometer. The above procedure was repeated for four sub-samples for each of the samples from the centre and the periphery of the core.

2.4 Extraction of cation exchanged Fe(II) on synthetic smectite

As a control, the exchanged Fe(II) extraction procedure was applied to a synthetic montmorillonite, whose exchanger composition had been enriched in Fe(II). 0.5 mL of a 0.005 mol L^{-1} $FeCl_2$ (purity grade) solution was introduced into a 4.5 mL synthetic montmorillonite suspension (30 g L^{-1}) previously equilibrated with a $CaCl_2$ 0.05 mol L^{-1} solute background. The resulting 5 mL of Fe-Ca montmorillonite suspension were then filtered on a 0.1 μm filter. Subsequently, the same Fe(II) extraction procedure as that used for the Callovian-Oxfordian sample was applied.

2.5 Extraction of cation exchanged Na, Ca, Mg, K and Sr

Cation exchanged Na, Ca, Mg, K and Sr were extracted using the cobalthexamine method as described in Gaucher et al., 2004, adapting the method from Ciesielski and Sterckeman, 1997.

2.6 Optical microscopic observations

Samples were observed on thin polished sections using a transmitted and reflected light optical microscope to identify transparent and opaque mineral phases.

2.7 Scanning electron microscopy

Observations, analyses and elemental mapping were performed with a JEOL JSM 6100 scanning electron microscope (SEM) coupled with an Energy Dispersive Spectrometer (Kevex Quantum) at 25 kV. Prior to analysis, a thin carbon layer was sputter-coated on the samples (Edwards Auto 306).

2.8 Transmission electron microscopy

Observations and analyses were performed at Orléans University (France), on a Philips CM20 with a CCD Gatan camera, at 200 kV. The TEM samples were prepared by dispersing the powdered samples in alcohol using ultrasonic treatment, dropping them onto a porous carbon film supported on a copper grid, and then drying them in air.

2.9 Electron microprobe

Spot analyses and elemental mapping were performed using a Camebax SX50 electron microprobe. Elemental mappings were recorded with a step of 4 μm , an acceleration voltage of 15 kV and a current beam of 14 nA. Spot analyses of silicates, carbonates, oxides and sulphates were performed with 15 kV acceleration voltage, a current beam of 12 nA and a 1-2 μm beam width. The counting time was 10 s for major elements and 20 s for trace elements. Standards used included both well-characterized natural minerals and synthetic oxides. Matrix corrections were made with a ZAF computing program. Detection limits of elements were calculated for carbonates (Table 1).

2.10 Mössbauer spectrometry

The Mössbauer sample holder was filled with about 300 mg of powder, capped and sealed with an AralditeTM epoxy resin in the glove box with a <0.1 ppm O_2 atmosphere. The Mössbauer sample was kept overnight in the glove box so that the epoxy resin could dry, and was then taken out and immediately reintroduced into the liquid- N_2 -filled Dewar for transport to the Mössbauer facilities. The Mössbauer spectra were recorded at 77 K using a constant acceleration spectrometer and a ^{57}Co source diffusing into a rhodium matrix. Velocity calibrations were carried out using α -Fe foil at room temperature (RT, 295 K). All isomer shifts are reported relative to the α -Fe spectrum obtained at RT.

The hyperfine structure clearly revealed the presence of ferric and ferrous ions from the central part and the right part, respectively. The spectra were first fitted using a discrete number of independent quadrupolar doublets composed of Lorentzian lines where the line width at half-height Γ (mm s^{-1}), the centre shift δ (mm s^{-1}) and the quadrupole splitting ΔE_Q (mm s^{-1}) were refined using a least-squared fitting procedure. However, it is important to emphasize that numerous fitting models can be used to describe the hyperfine structure.

Consequently, different quadrupolar hyperfine parameters were chosen in a second stage amongst those available in the literature (e.g. in Stevens et al., 2005) for the identified phase by microscopic techniques in the samples and vice-versa. Finally, only the proportions of each Fe component were refined, thereby allowing a quantitative analysis of the sample.

3. Experimental results

3.1 Extraction of exchanged Fe on synthetic montmorillonite

A Fe concentration of 9×10^{-6} mol L⁻¹ was recovered in the filtrate, corresponding to an exchanged content of 6.8 meq kg⁻¹, according to the following equation:

$$C_{FeX_2} = 2 \times \frac{C_{filtrate} \times V}{m_{clay}} \quad \text{Equation 1}$$

where $C_{filtrate}$ is the Fe(II) concentration in the filtrate in mol L⁻¹, V is the volume of the filtrate (5 mL) and m_{clay} is the mass of clay on the filtrate (0.135 g).

This extracted Fe(II) content compares well with the expected content, 6.9 meq kg⁻¹, as given by the cation exchange capacity of the clay (0.63 eq kg⁻¹, Gehin et al., 2007) and the Fe(II) cation exchange model by Charlet and Tournassat, 2005. We consider that this test validates our method of exchanged Fe extraction and that our protocol enables at least the exchanged Fe(II) content of the clay material to be recovered.

Kinetics tests were also carried out and clearly showed a readsorption of the complex Fe-phenanthroline with increasing reaction time (data not shown). The filtration duration conditions given in the Materials and Methods section aims at minimizing this effect.

3.2 Exchanged Fe(II) on Callovian-Oxfordian claystone samples

Table 2 shows the extracted Fe(II) content for the two samples, centre and periphery. It may be noted that the recovered amount in the centre is higher than in the periphery. There are two main hypotheses to explain this discrepancy:

- The mineralogical composition was enriched in clay in the core centre sample as compared to the periphery sample, leading to a greater extent of exchanged Fe in the centre sample;
- Oxidation occurred during drilling or during crushing of the periphery sample.

Whatever the cause of this discrepancy, the measured exchanged Fe is of the order of magnitude of 1 meq/kg rock in these samples. In the following, the centre sample with mean extracted Fe content of 1.2 ± 0.2 meq kg⁻¹ will be considered. This extracted Fe(II) must be considered as the upper limit of cation exchanged Fe(II) concentration in the clay sample. It has already been shown that Fe(II) can sorb specifically on clay edges and that most of this sorbed Fe(II) is present as weakly bounded outer-sphere complexes at pH above ~7 (Gehin et al., 2007). Given the near neutral pH of the porewater in the Callovian-Oxfordian samples (Gaucher et al., 2006), part of the extracted Fe(II) is then expected to originate from the clay edges.

3.3 Other exchanged cations in the samples

Table 3 shows the extracted exchanged Na, K, Ca, Mg and Sr contents for the two samples, centre and periphery. The exchanged contents of Na, K, Ca, Mg and Sr are very similar in the centre and periphery samples. The first hypothesis given above for the variability of exchanged Fe is then ruled out. The relative proportions between exchanged Na, K, Ca and Mg compare well with previously reported data on Callovian-Oxfordian samples (Gaucher et al., 2004), highlighting the homogeneity of the clay formation towards cation exchange processes.

3.4 Microscopic and spectrometric observations of Fe bearing minerals

Iron is distributed among numerous phases of the Callovian-Oxfordian clay samples: silicates, carbonates, sulphur phases and oxides (Table 4). Silicates include dominantly detrital clay minerals (illite, interstratified illite-smectite and chlorite), minor detrital micas (biotite, muscovite), scarce detrital tourmaline and local diagenetic glauconite (Figure 1). Carbonates include dominantly calcite with minor iron-bearing dolomite, ankerite and siderite (Figures 2 and 3). Calcite constitutes a large part of the fine-grained matrix with clay minerals, but also occurs as rare euhedral 50-100 μm -sized grains. Dolomite and ankerite occur respectively as core and rims of euhedral 50-100 μm -sized grains in most of the samples of the Callovian-Oxfordian formation (Figure 2C). Siderite is present as rims of euhedral 50-100 μm -sized grains, growing after iron-rich calcite in the sample EST 25687 (Figure 2D).

Sulphides are syn-sedimentary to diagenetic, dominantly pyrite and scarce iron-bearing sphalerite. Iron can be found also in detrital ilmenite (Fe(II)TiO_3). It should be noted that diagenetic minerals are particular iron-rich mineral phases (glauconite, pyrite, ankerite and siderite).

Taking account of the distribution of the different mineral phases in the Callovian-Oxfordian rocks, the iron is mainly carried in decreasing order by detrital clay minerals, sedimentary to diagenetic pyrite and sedimentary calcite. Diagenetic siderite is one of the main iron carrier minerals in one observed sample (EST 25687). This iron distribution in the different mineral phases of the Callovian-Oxfordian claystone is further supported by the 77K Mössbauer spectrum of the EST 25687 sample (Figure 4, Table 5): the Mössbauer spectrum can be perfectly reproduced using only quadrupolar doublets parameters of the phases identified by the microscopic techniques. Mössbauer spectrometry results indicate that the redox state of Fe in the formation is mainly Fe(II). The reported 7% of Fe(III) is the maximum relative amount that can be introduced into the fitting model.

3.5 Microscopic and spectrometric observations of Sr bearing minerals

Strontium is a trace element in the Callovian-Oxfordian formations (0.025-0.12% wt % SrO, Gaucher et al., 2004). Contrary to iron, it is essentially carried by one phase, namely celestite (SrSO_4), and is present at only trace concentrations in carbonates. The celestite precipitated in late infilling of porosity and in veins, and is therefore a diagenetic mineral phase. Compositions of iron-rich dolomite and ankerite were analyzed in the rims of euhedral grains disseminated in the rocks or associated with celestite, suggesting that iron-rich dolomite and ankerite are also diagenetic mineral phases. The strontium content in carbonate phases is low, generally below 0.09 wt % SrO, except late calcite overprinting celestite vein and some euhedral grains of dolomite that exhibit a strontium content up to 0.6 wt % SrO.

4. Discussion

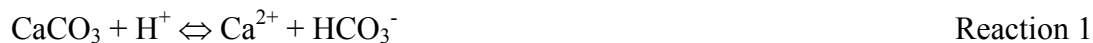
4.1 Estimation of carbonate mineral solubility values with cation exchange composition

The exchanger composition of a clay rock provides information about the relative amount of exchanged cations, namely Na^+ , K^+ , Ca^{2+} , Mg^{2+} , but also Sr^{2+} and Fe^{2+} , in solution through exchange equilibrium reactions (Tournassat et al., 2007). As already described in the literature, the exchanger composition is then an “image” of the porewater major cation composition (Bradbury and Baeyens, 1998; Gaucher et al., 2006; Pearson et al., 2003).

This porewater composition is also in equilibrium with mineral phases. The consideration of these equilibria is the basis of porewater model development (e.g. Gaucher et al., 2006). Based on microscopic and spectrometric observations (this study, Gaucher et al., 2004; Gaucher et al., 2006), it is likely that the COX porewater is in equilibrium with the following carbonate minerals: calcite, dolomite and ankerite/siderite, but not with strontianite (SrCO_3).

Hence, the following equilibria must apply:

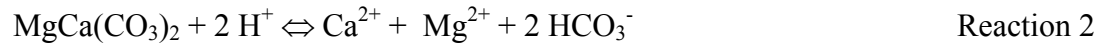
- Calcite dissolution/precipitation:



$$K_{\text{calcite}} = \frac{\{Ca^{2+}\}\{HCO_3^-\}}{\{H^+\}} \quad \text{Equation 2}$$

where values in brackets are representative of solute species activities.

- Dolomite dissolution/precipitation:



$$K_{\text{dolomite}} = \frac{\{Ca^{2+}\}\{Mg^{2+}\}\{HCO_3^-\}^2}{\{H^+\}^2} \quad \text{Equation 3}$$

- Siderite dissolution/precipitation:



$$K_{\text{siderite}} = \frac{\{Fe^{2+}\}\{HCO_3^-\}}{\{H^+\}} \quad \text{Equation 4}$$

Combining Equation 2 with Equation 3, one obtains:

$$\frac{K_{\text{dolomite}}}{K_{\text{calcite}}^2} = \frac{\{Mg^{2+}\}}{\{Ca^{2+}\}} \quad \text{Equation 5}$$

The Mg/Ca solute activity ratio is also linked to cation exchange equilibrium:



$$K_{ex}^{Ca/Mg} = \frac{\{Ca^{2+}\}}{\{Mg^{2+}\}} \times \frac{E_{MgX_2}}{E_{CaX_2}} \quad \text{Equation 6}$$

where K_{ex} is the exchange selectivity coefficient in the Gaines and Thomas convention (Sposito, 1981), X represents one mole of the exchanger and E_i is the exchanged equivalent fraction of species i .

Combining Equations 5 and 6:

$$K_{dolomite} = K_{calcite}^2 \times \frac{E_{MgX_2}}{E_{CaX_2} \times K_{ex}^{Ca/Mg}} \quad \text{Equation 7}$$

With siderite, one obtains:

$$K_{siderite} = K_{calcite} \times \frac{E_{FeX_2}}{E_{CaX_2} \times K_{ex}^{Ca/Fe}} \quad \text{Equation 8}$$

The exchanger composition is then directly related to the equilibrium constant of calcite, dolomite and siderite carbonate minerals. While the calcite equilibrium constant is well constrained, that is not the case for dolomite. The above equations are then useful for constraining the carbonate equilibrium constant in natural systems. For siderite, unfortunately, the value E_{FeX_2} is not known exactly: the extracted Fe(II) measurements in the above experiments ($E_{FeX_2}^{meas}$) give only an indication of its maximum amount and then:

$$K_{siderite} < K_{calcite} \times \frac{E_{FeX_2}^{meas}}{E_{CaX_2} \times K_{ex}^{Ca/Fe}} \quad \text{Equation 9}$$

Strontianite was never observed in fresh Callovian-Oxfordian samples. It means that the porewater is likely to be undersaturated towards this mineral phase. The equalities given above cannot be used to determine the strontianite solubility value. However, the absence of strontianite in the formation can be related in the equation form:

$$K_{\text{strontianite}} > K_{\text{calcite}} \times \frac{\{Sr^{2+}\}}{\{Ca^{2+}\}} \quad \text{Equation 10}$$

Combining Equation 10 with the information from cation exchange:

$$K_{\text{strontianite}} > K_{\text{calcite}} \times \frac{E_{SrX_2}}{E_{CaX_2} \times K_{ex}^{Ca/Sr}} \quad \text{Equation 11}$$

4.2 Dolomite, siderite and strontianite equilibrium constants

There is a good agreement between the thermodynamic databases available in the literature and provided with thermodynamic calculation codes for calcite thermodynamic parameters. Most of these databases rely on the calcite data by Plummer and Busenberg, 1982. For reaction 1, the calcite solubility value is $\log_{10} K_{\text{calcite}} = 1.85$.

As a consequence, we used the $\log_{10} K_{\text{calcite}} = 1.85$ as a reference point for the calculation of the solubility value of dolomite and siderite in the clay formation using the following formulas:

$$\log_{10} K_{\text{dolomite}} = 2 \times \log_{10} K_{\text{calcite}} + \log_{10} E_{MgX_2} - \log_{10} K_{ex}^{Ca/Mg} - \log_{10} E_{CaX_2} \quad \text{Equation 12}$$

$$\log_{10} K_{siderite} < \log_{10} K_{calcite} + \log_{10} E_{FeX_2}^{meas} - \log_{10} K_{ex}^{Ca/Fe} - \log_{10} E_{CaX_2} \quad \text{Equation 13}$$

For strontianite one obtains:

$$\log_{10} K_{strontianite} > \log_{10} K_{calcite} + \log_{10} E_{SrX_2} - \log_{10} K_{ex}^{Ca/Sr} - \log_{10} E_{CaX_2} \quad \text{Equation 14}$$

Ca and Mg are known to behave very similarly on smectite and illite exchanger with little preference for Ca over Mg (smectite exchanger, Charlet and Tournassat, 2005; Sposito et al., 1983a; Sposito et al., 1983b) or little preference (illite exchanger, Tournassat et al., 2007) for Mg over Ca. Hence, we assume a $\log_{10} K_{ex}^{Ca/Mg}$ value of 0. Fe and Ca behave similarly towards cation exchange and we assume here a \log_{10} of the selectivity coefficient equal to 0 (Charlet and Tournassat, 2005; Kamei et al., 1999; Saeki et al., 2004). The same assumption is made for the Ca/Sr exchange selectivity coefficient (Fletcher and Sposito, 1989). The obtained solubility values are compared in Table 6 to the one tabulated in various databases especially available with thermodynamic calculation codes.

In NAGRA/PSI, Minteq.v4 and Wateq4f (the one distributed with GWB, not with PHREEQC2), the original equilibrium constant value, 3.57, comes from the database published by Nordstrom et al. (Nordstrom et al., 1990). In a more recent determination, Hemingway and Robie (Hemingway and Robie, 1994) determined the Gibbs energy of formation by calorimetry, leading to the same value for the equilibrium constant, 3.57. The dolomite solubility value derived from the analysis of the cation exchange population of the Callovian-Oxfordian sample is about 3.3-3.4 in \log_{10} scale. This value compares well with the 3.57 value. The difference in value could be seen as (1) an effect of the error bands on cation exchange measurement or (2) an effect of temperature, the Callovian-Oxfordian formation

temperature being below 298K, (3) an effect of the impurities in the dolomite structure (e.g. Fe and Sr), or (4) the dissolution of calcite during the extraction procedure leading to an overestimation of Ca concentration on the exchanger phase (Dohrmann, 2006a; Dohrmann, 2006b; Dohrmann, 2006c). It should then be noted that the solubility value given in the Llnl.dat and derived database (e.g. Thermo.dat) cannot be applied to the clay media of the Callovian-Oxfordian (2 log K values depending on the crystallinity at values 2.51 and 4.06). The 4.06 value would be obtained in the case of an exchanged Mg/Ca ratio value of 2.3 instead of 0.48 ± 0.12 and the 2.51 value in the case of a ratio value of 0.065. Clearly none of these ratio values is relevant even considering the source of uncertainties in the measured ratio. It is then considered that the dolomite solubility value given by Nordstrom et al. is the best estimate of the one that applies to the Callovian-Oxfordian formation.

With regards to strontianite, very different values can be found as a function of the databases given in Table 6. The only value compatible with the constraint of Equation 11 is the solubility value of 1.06 that originates from the work of Busenberg et al., 1984.

The maximum siderite solubility value computed from extracted exchanged Fe(II) is in agreement with all of the solubility values of all the databases given in Table 6 with the exception of the Minteq.v4 database, which gives a too high solubility value.

The composition of the Fe(II) carbonate in the COX formation is not a pure siderite (FeCO_3) but a sideroplesite having a composition of approximately $\text{Fe}_{0.7}\text{Mg}_{0.2}\text{Ca}_{0.1}\text{CO}_3$ (see Figure 3) with a solubility product value of $\log K_{\text{sid_COX}}$. Using the same method as described above, one derives for this particular composition:

$$\log K_{\text{sid_COX}} < 0.6 \times \log K_{\text{calcite}} + 0.2 \times \log K_{\text{dolomite}} + 0.7 \times \log E_{\text{FeX}_2}^{\text{meas}} - 0.7 \times \log E_{\text{CaX}_2} - 0.7 \times \log K_{\text{ex}}^{\text{Ca/Fe}}$$

Equation 15

i.e., $\log K_{\text{sid_COX}} < 0.42$ when considering $\log K_{\text{calcite}} = 1.85$ and $\log K_{\text{dolomite}} = 3.57$.

The solubility product of a carbonate phase with the composition $\text{Fe}_{0.7}\text{Mg}_{0.2}\text{Ca}_{0.1}\text{CO}_3$ was evaluated using a ternary solid-solution model and the following three end-members: calcite, siderite and magnesite (MgCO_3). The solubility of calcite was taken from Plummer and Busenberg, 1982, that of siderite from Chivot, 2004, whereas that of magnesite was calculated from the ΔH°_f and S° values tabulated in Robie and Hemingway, 1995 for a natural magnesite.

The calculation of the free energy of mixing at 298 K (ΔG_{mix}) was obtained through the following relationships:

$$\Delta G_{mix} = R.T. \sum_{i=1}^3 X_i \ln X_i + \Delta G_{mix}^{excess} \quad \text{Equation 16}$$

$$\Delta G_{mix}^{excess} = X_1 X_2 W_{12} + X_1 X_3 W_{13} + X_2 X_3 W_{23} + X_1 X_2 X_3 W_{123} \quad \text{Equation 17}$$

where R is the gas constant ($8.314 \text{ J mol}^{-1} \text{ K}^{-1}$), T the temperature in K (298 K), X_i is the molar fraction of end member i (1, 2, 3 representative of calcite, magnesite and siderite respectively), ΔG_{mix}^{excess} is the excess free energy of mixing and $W_{ij(k)}$ are interaction parameters. For reasons of simplicity, we used the Davies and Navrotsky formulation for regular solid-solution (Davies and Navrotsky, 1983, Eq. 26). The binary terms (W_{ij}) were estimated using the model given in Davies and Navrotsky, 1983: $W_{cs} = 20.2 \text{ kJ mol}^{-1}$, $W_{cm} = 23.9 \text{ kJ mol}^{-1}$ and $W_{ms} = 4.3 \text{ kJ mol}^{-1}$ where subscripts c, s and m refer to calcite, siderite and magnesite respectively. The ternary term W_{cms} was neglected owing to the lack of available parameters to estimate its value. W_{ms} value is low and is in agreement with the continuous domain of miscibility between the magnesite and the siderite end-members at 25°C. Furthermore, the estimated value is in close agreement with the value measured by Chai and Navrotsky, 1996, namely $4.44 \pm 0.75 \text{ kJ mol}^{-1}$. W_{cm} and W_{cs} values are high in agreement with

the presence of a large miscibility gap between calcite and magnesite or calcite and siderite end-members (Ganguly and Saxena, 1987).

Considering these parameters, we could estimate the solubility of sideroplesite as $\log K_{sid_COX} = 0.23$. This value is in agreement with the constraint obtained with the clay cation exchanger composition. Nevertheless, several sources of uncertainties in this calculation need to be highlighted: (i) the model was performed with estimated and not measured W parameters, (ii) a regular solid-solution model was used, and (iii) the ternary mixing term was neglected. In addition, the considered composition is a “bulk” composition of the grain rim and could be non-representative of the composition in contact with the porewater. Further spectroscopic experiments are planned to refine this preliminary model.

5. Conclusions

The microscopic and spectrometric investigations of Fe and Sr bearing phases and the relationship between cation exchanger composition and carbonate solubility products enabled the following conclusions to be drawn:

- The solubility product of dolomite in the COX formation is in agreement with the one determined by Hemingway and Robie, 1994 ($\log K_{dolomite} = 3.57$);
- The only solubility product of strontianite that agrees with the exchanger composition and the absence of this mineral phase from the Callovian-Oxfordian formation is the one determined by Busenberg et al., 1984 ($\log K_{strontianite} = 1.06$);
- A preliminary solubility product has been estimated for the siderite like mineral present in the EST 25687 sample: $Fe_{0.7}Mg_{0.2}Ca_{0.1}CO_3 + H^+ \Leftrightarrow 0.7 Fe^{2+} + 0.2 Mg^{2+} + 0.1 Ca^{2+} + HCO_3^-$ $\log K_{sid_COX} = 0.23$.

Furthermore, the very homogeneous cation exchange composition relative to Ca and Mg of the formation is completely linked to a homogeneous presence of calcite and dolomite minerals, whose equilibrium reactions control part of the porewater composition. Given the ubiquitous presence of siderite/ankerite minerals in the formation, we anticipate that the exchangeable Fe/Ca ratio of the sample EST 25687 is also valid in the whole COX formation. Unfortunately, the value obtained in this paper must be considered only as an upper limit for this ratio, i.e. about 0.01.

With regards to Fe(III) oxi(hydr)oxide mineral phases, it is now clear that they are absent from the COX samples that were well preserved from oxidation by atmospheric O₂.

The consideration of mineral-water and cation exchange equilibria is the basis of the porewater composition estimation models previously published in the literature (Bradbury and Baeyens, 1998; Coudrain-Ribstein and Gouze, 1993; Gaucher et al., 2006; Pearson et al., 2003). The present study, together with on-going URL experiments (Vinsot and Delay, 2007 (accepted)) and new data acquisitions, will help to refine these models, particularly for the redox control of the porewater. Future models and associated thermodynamic databases must, at least, lead to the following results: equilibrium with a sideroplesite or ankerite mineral, equilibrium with pyrite and overall undersaturation with regards to ferrihydrite, goethite, magnetite and hematite.

Acknowledgements

This research has been financially supported by the 6th PCRD Euratom FUNMIG program and the BRGM-ANDRA scientific partnership. Claire Beny, Fabian Delorme and Christian Gilles are acknowledged for their help with SEM, TEM and electron microprobe analyses.

We would like to thank Agnès Vinsot (ANDRA URL, Bure, PI of the PAC experiments) for providing access to core samples under good conditions with regard to oxidation preservation.

References

- ANDRA, 2005. Référentiel du comportement des radionucléides et des toxiques chimiques d'un stockage dans le Callovo-Oxfordien jusqu'à l'Homme. Dossier 2005 Argile, Agence Nationale pour la gestion des déchets radioactifs, Châtenay-Malabry, France.
- Bethke, C.M., 1996. Geochemical reaction modeling. Oxford University Press.
- Bradbury, M.H. and Baeyens, B., 1998. A Physicochemical characterisation and geochemical modelling approach for determining porewater chemistries in argillaceous rocks. *Geochim. Cosmochim. Acta*, 62(5): 783-795.
- Busenberg, E., Plummer, L.N. and Parker, V.B., 1984. The solubility of strontianite (SrCO_3) in CO_2 - H_2O solutions between 2 and 91°C, the association constants of $\text{SrHCO}_3^+(\text{aq})$ and $\text{SrCO}_3^0(\text{aq})$ between 5 and 80°C, and an evaluation of the thermodynamic properties of $\text{Sr}^{2+}(\text{aq})$ and $\text{SrCO}_3(\text{cr})$ at 25°C and 1 atm total pressure. *Geochim. Cosmochim. Acta*, 48(10): 2021-2035.
- Chai, L. and Navrotsky, A., 1996. Synthesis, characterization, and enthalpy of mixing of the (Fe,Mg) CO_3 solid solution. *Geochim. Cosmochim. Acta*, 60(22): 4377-4383.
- Charlet, L. and Tournassat, C., 2005. Fe(II)-Na(I)-Ca(II) cation exchange on montmorillonite in chloride medium; evidence for preferential clay adsorption of chloride – metal ion pairs in seawater. *Aquat. Geoch.*, 11(2): 115-137.
- Chivot, J. (Editor), 2004. Fonctions thermodynamiques, diagrammes de solubilité, diagrammes E-pH des systèmes Fe- H_2O , Fe- CO_2 - H_2O , Fe-S- H_2O , Cr- H_2O et Ni- H_2O en fonction de la température. Thermodynamique des produits de corrosion. ANDRA, Châtenay-Malabry, France.
- Ciesielski, H. and Sterckeman, T., 1997. Determination of cation exchange capacity and exchangeable cations in soils by means of cobalt hexamine trichloride. *Effects of experimental conditions. Agronomie*, 17: 1-7.
- Coudrain-Ribstein, A. and Gouze, P., 1993. Quantitative study of geochemical processes in the Dogger aquifer, Paris Basin, France. *Appl. Geochem.*, 8(5): 495-506.
- Davies, P.K. and Navrotsky, A., 1983. Quantitative correlations of deviations from ideality in binary and pseudobinary solid solutions. *J. Solid State Chem.*, 46: 1-22.
- Dohrmann, R., 2006a. Cation exchange capacity methodology I: An efficient model for the detection of incorrect cation exchange capacity and exchangeable cation results. *Applied Clay Science*, 34(1-4): 31-37.
- Dohrmann, R., 2006b. Cation exchange capacity methodology II: A modified silver-thiourea method. *Applied Clay Science*, 34(1-4): 38-46.
- Dohrmann, R., 2006c. Cation exchange capacity methodology III: Correct exchangeable calcium determination of calcareous clays using a new silver-thiourea method. *Applied Clay Science*, 34(1-4): 47-57.
- Fletcher, P. and Sposito, G., 1989. The chemical modeling of clay/electrolyte interactions for montmorillonite. *Clay Miner.*, 24: 375-391.
- Ganguly, J. and Saxena, S.K., 1987. Mixtures and mineral reactions. *Minerals and rocks*. Springer-Verlag, Heidelberg.

- Gaucher, E., Robelin, C., Matray, J.M., Negrel, G., Gros, Y., Heitz, J.F., Vinsot, A., Rebours, H., Cassabagnere, A. and Bouchet, A., 2004. ANDRA underground research laboratory: Interpretation of the mineralogical and geochemical data acquired in the Callovian-Oxfordian Formation by investigative drilling. *Physics and chemistry of the earth*, 29(1): 55-77.
- Gaucher, E.C., Blanc, P., Bardot, F., Braibant, G., Buschaert, S., Crouzet, C., Gautier, A., Girard, J.-P., Jacquot, E., Lassin, A., Negrel, G., Tournassat, C., Vinsot, A. and Altmann, S., 2006. Modelling the porewater chemistry of the Callovian-Oxfordian formation at a regional scale. *C.R. Geosci.*, 338(12-13): 917-930.
- Gehin, A., Greneche, J.-M., Tournassat, C., Brendle, J., Rancourt, D.G. and Charlet, L., 2007. Reversible surface-sorption-induced electron-transfer oxidation of Fe(II) at reactive sites on a synthetic clay mineral. *Geochim. Cosmochim. Acta*, 71(4): 863-876.
- Girard, J.-P., Flehoc, C. and Gaucher, E., 2005. Stable isotope composition of CO₂ outgassed from cores of argillites: a simple method to constrain $\delta^{18}\text{O}$ of porewater and $\delta^{13}\text{C}$ of dissolved carbon in mudrocks. *Appl. Geochem.*, 20(4): 713-725.
- Hemingway, B.S. and Robie, R.A., 1994. Enthalpy and Gibbs energy of formation of dolomite, CaMg(CO₃)₂, at 298.15 K from HCl solution calorimetry. U.S. Geol. Surv. Open-file report 94-575.
- Hummel, W., Berner, U.R., Curti, E., Pearson, F.J. and Thoenen, T., 2002. NAGRA/PSI chemical thermodynamic data base 01/01. Universal Publishers/uPublish.com, Parkland, Florida.
- Kamei, G., Oda, C., Mitsui, S., Shibata, M. and Shinozaki, T., 1999. Fe(II)-Na ion exchange at interlayers of smectite: adsorption-desorption experiments and a natural analogue. *Eng. Geol.*, 54: 15-20.
- Michel, P., Lerouge, C., Gaucher, E.C. and Tournassat, C., 2006. Report on meshing for the transport model in the Callovian-Oxfordian formation, Reports of the FP6 European Euratom program FUNMIG (FP6-516514).
- Nordstrom, D.K., Plummer, L.N., Langmuir, D., Busenberg, E., May, H.M., Jones, B.F. and Parkhurst, D.L., 1990. Revised chemical equilibrium data for major water-mineral reactions and their limitations. In: R.L. Bassett and D. Melchior (Editors), *Chemical modeling in aqueous systems II*. American Chemical Society Symposium Series 416, Washington D.C., pp. 398-413.
- Parkhurst, D.L. and Appelo, C.A.J., 1999. User's guide to phreeqc - a computer program for speciation, batch-reaction, one-dimensional transport, and inverse geochemical calculations. 99-4259, U.S. Geological Survey, Denver (Colorado).
- Pearson, F.J., Arcos, D., Boisson, J.-Y., Fernandez, A.M., Gäbler, H.-E., Gaucher, E., Gautschi, A., Griffault, L., Hernan, P. and Waber, H.N. (Editors), 2003. Mont Terri project - Geochemistry of water in the Opalinus clay formation at the Mont Terri Rock Laboratory. *Geology Series*, 5, Bern.
- Plummer, L.N. and Busenberg, E., 1982. The solubilities of calcite, aragonite and vaterite in CO₂-H₂O solutions between 0 and 90[degree sign]C, and an evaluation of the aqueous model for the system CaCO₃-CO₂-H₂O. *Geochim. Cosmochim. Acta*, 46(6): 1011-1040.
- Reinholdt, M., Miéché-Brendlé, J., Delmotte, L., Tuillier, M.-H., de Dred, R., Cortès, R. and Flank, A.-M., 2001. Fluorine route synthesis of montmorillonites containing Mg or Zn and characterization by XRD, thermal analysis, MAS NMR, and EXAFS spectroscopy. *Eur. J. Org. Chem.*, 2001: 2831-2841.
- Robie, R.A. and Hemingway, B.S., 1995. Thermodynamic properties of minerals and related substances at 298.15 K and 1 bar (10⁵ Pascals) pressure and a higher temperatures. Bulletin 2131, United States Government Printing Office, Washington.

- Rodier, J., 1996. L'Analyse de l'eau, eaux naturelles, eaux résiduaires, eau de mer. Dunod, Paris, 1384 pp.
- Saeki, K., Wada, S.-I. and Shibata, M., 2004. Ca^{2+} - Fe^{2+} and Ca^{2+} - Mn^{2+} exchange selectivity of kaolinite, montmorillonite, and illite. *Soil Sci.*, 169(2): 125-132.
- Sposito, G., 1981. The thermodynamics of soil solution. Oxford University Press, New York.
- Sposito, G., Holtzclaw, K.M., Jouany, C. and Charlet, L., 1983a. Cation selectivity in sodium-calcium, sodium-magnesium, and calcium-magnesium exchange on Wyoming bentonite at 298 K. *Soil Sci. Soc. Am. J.*, 47(5): 917-921.
- Sposito, G., Jouany, C., Holtzclaw, K.M. and LeVesque, C.S., 1983b. Calcium-Magnesium exchange on Wyoming bentonite in the presence of adsorbed sodium. *Soil Sci. Soc. Am. J.*, 47: 1081-1085.
- Stevens, J.G., Khasanov, A.M., Miller, J.W., Pollak, H. and Li, Z., 2005. Mössbauer Mineral Handbook. MEDC.
- Tournassat, C., Gailhanou, H., Crouzet, C., Braibant, G., Gautier, A., Lassin, A., Blanc, P. and Gaucher, E.C., 2007. Two cation exchange models for direct and inverse modelling of solution major cation composition in equilibrium with illite surfaces. *Geochim. Cosmochim. Acta*, 71(5): 1098-1114.
- Vinsot, A. and Delay, J., 2007 (accepted). In situ sampling and characterization of Callovo-Oxfordian pore water, Proceedings of the Water Rock Interaction conference, Vol.

Figure captions

Figure 1. Optical microscopic observations using transmitted natural light. A, B and D: sample EST 25380; C: sample EST 25687. Glt: glauconite; Bt: biotite; Ms: muscovite; Chl: chlorite; Tur: tourmaline. *(Intended for colour reproduction in print)*

Figure 2. A: Micrograph of pyrite (Py) and sphalerite (Sph) (backscattered electron image – sample 12436); B: Macrograph of a celestite vein crosscutting the Callovian-Oxfordian formation (Sample EST 20714); Micrograph of an euhedral grain of dolomite with an iron-rich rim (backscattered electron image – sample EST 21400); D: Micrograph of an euhedral grain of carbonate. The core is an iron-rich calcite (Cc), whereas the rim is a siderite (Sd) (backscattered electron image – sample EST 25687). *(Intended for colour reproduction in print)*

Figure 3. Triangular Ca-Fe-Mg diagram showing the main chemical compositions of the carbonates in the Callovian-Oxfordian formations. Black symbols correspond to the sample EST 25687 in which siderite grew after iron-rich calcite. Open symbols correspond to all other samples.

Figure 4. 77 K Mössbauer spectrum of sample EST 25687. Red, pink, green, light blue and dark blue curves refer to Mössbauer fitting components given in Table 5. The black curve is the sum of all of these contributions. *(Intended for colour reproduction in print)*

Table 1. Detection limits of Ba, Ca, Fe, Mg, Mn and Sr in carbonates using electron microprobe analysis.

Elements	BaO	CaO	FeO	MgO	MnO	SrO
Detection limits wt %						
oxides	0.11	0.08	0.07	0.02	0.07	0.02

Table 2. Results of the extraction of Fe exchanged on COX samples (EST25687). The “centre” sample was very well preserved from oxidation by the air, whereas the “periphery” one was more subject to O₂ exposure.

Location of the sample in the core	Replicate number	Exchanged Fe (meq/kg)
Centre	#1	1.4
	#2	1.4
	#3	1.1
	#4	0.7
Periphery	#1	0.9
	#2	0.3
	#3	0.4
	#4	0.4

Table 3. Na, K, Ca, Mg and Sr contents exchanged by the cobalthexamine method (Ciesielski and Sterckeman, 1997) on the “centre” and “periphery” samples (EST25687).

Location of the sample in the core	Replicate number	Exchanged Cations (meq/kg)				
		Na	K	Ca	Mg	Sr
Centre	#1	36	14	103	39	5
	#2	38	15	107	39	5
	#3	38	15	109	41	5
Periphery	#1	37	14	106	42	5
	#2	35	13	98	40	5
	#3	38	14	109	44	5

Table 4. List of Fe-bearing minerals in the Callovian-Oxfordian clay rocks, their formation, their percentage in the rock, their general chemical composition and their average iron content given in weight percent of FeO. The * indicates an exceptional high iron content analyzed in the calcite of only one sample of the Callovian-Oxfordian formations (EST 25687). n.d. = not determined (below quantification limit).

		Indicative % of phases in COX samples	Structural formulae	Eq. wt% FeO
Silicates				
Biotite	detrital	traces	$K_2 (Fe, Mg)_{6-4} (Fe, Al, Ti)_{0-2} (Si_{6.5} Al_{2.3} O_{20}) (OH, F)_4$	13 - 22
Chlorite	detrital	~ 2 %	$(Fe, Mg Al)_{12} ((Si, Al)_8 O_{20}) (OH)_{16}$	~ 20
Muscovite/phengite	detrital	traces	$(K, Na)_2 (Fe, Mg, Fe, Al, Ti) (Si_{6.4} Al_{1.6} O_{20}) (OH)_4$	1 - 3
Dioctahedral interlayer-deficient micas	detrital	36-71	$(K, Na)_{x+y} (Fe^{2+}, Mg)_x (Fe^{3+}, Al)_{2-x} (Si_{4-y} Al_y O_{10}) (OH)_2 nH_2O$	1.7 - 5.7
Glauconite	diagenetic	n.d.	$(K)_{0.8} (Fe^{2+}, Fe^{3+}, Mg, Al)_4 (Si_{7-7.6} Al_{1-0.4} O_{20}) (OH)_4 nH_2O$	9.3 - 16.5
Tourmaline	detrital	n.d. (<1 %)	$(K, Na) (Fe, Mg, Li, Al)_3 Al_6 (Si_6 O_{18}) (BO_3)_3 (OH, F)_4$	6.2-10.6
Carbonates				
Calcite cement	sedimentary	15-95	$CaCO_3$	0.2 - 0.8
Core of euhedral calcite	detrital or sedimentary	n.d.		< 0.5 4 - 6 *
Calcite II	diagenetic	n.d.		0.1 - 3.2
Iron rich dolomite II/ankerite	diagenetic	< 10 %	$Ca (Mg, Fe) (CO_3)_2$	0.1 - 6.0-14.4
Siderite	diagenetic	< 5 %	$FeCO_3$	41
Fe(II) -Ti-Oxide				
Ilmenite	detrital	n.d. (<1 %)	$FeTiO_3$	19 - 29
Sulphides				
Pyrite	sedimentary to diagenetic	0.2-3	FeS_2	52 - 53
Sphalerite	sedimentary to diagenetic	n.d. (<1 %)	ZnS	0.8-10.9

Table 5. Mössbauer parameters of sample EST 25687 at 77 K. I.S. = Isomer shift value relative to that of the α -Fe at 300 K; Γ = line width; Q.S. = quadrupolar splitting value; % = ratio of each component.

		I.S. mm s ⁻¹	Γ mm s ⁻¹	Q.S. mm s ⁻¹	%	Doublet structural attributions
EST 25687 sample	Doublet 1 (red)	0.40	0.34	0.61	39%	Fe(II) in pyrite
	Doublet 2 (light blue)	1.40	0.41	2.14	15%	Fe(II) in carbonates
	Doublet 3 (dark green)	1.31	0.28	3.02	20%	Fe(II) associated with clay minerals (structural and/or sorbed iron)
	Doublet 4 (pink)	1.20	0.27	3.02	19%	
	Doublet 5 (blue)	0.40	0.56	0.45	2%	Fe(III) associated with clay minerals
	Doublet 6 (green)	0.40	0.38	1.10	5%	

Table 6. Comparison of computed dolomite, siderite and strontianite solubility values with tabulated values in databases available in the literature.

	Solubility value (\log_{10})				
	Dolomite (ordered)	Dolomite (disordered)	Siderite	FeCO ₃ (pr)	Strontianite
This study, sample EST 25687, 6 experimental points	3.29 ± 0.02		< -0.11 ± 0.10		> 0.55
This study, data from (a), 29 experimental points at different depths	3.44 ± 0.04		N.A		N.A.
This study, data from (b), 128 experimental points at different depths	3.36 ± 0.13		N.A		N.A.
NAGRA-PSI (c)	3.57	4.12	-0.56	-0.12	1.06
Llnl.dat (d)	2.51	4.06	-0.19		-0.31
Minteq.v4.dat (d,e,f)	3.57	4.12	0.09		1.06
Wateq4f.dat (d)	4.12		-0.56		1.06
Wateq4f.dat (e)	3.57		-0.56	-0.12	1.06
Thermo.dat (e)	2.52	4.06	-0.22		-1.08
Chivot (g)			-0.47		

(a) Gaucher et al., 2004.

(b) Michel et al., 2006

(c) Hummel et al., 2002, available at <http://les.web.psi.ch/TDBbook/index.htm>.

(d) Provided with PHREEQC2, http://wwwbrr.cr.usgs.gov/projects/GWC_coupled/phreeqc/, Parkhurst and Appelo, 1999.

(e) Provided with The Geochemist's Workbench (GWB), (Bethke, 1996), http://www.geology.uiuc.edu/Hydrogeology/hydro_thermo.htm.

(f) Provided with Visual Minteq, <http://www.lwr.kth.se/English/OurSoftware/vminteq/>.

(g) Chivot, 2004

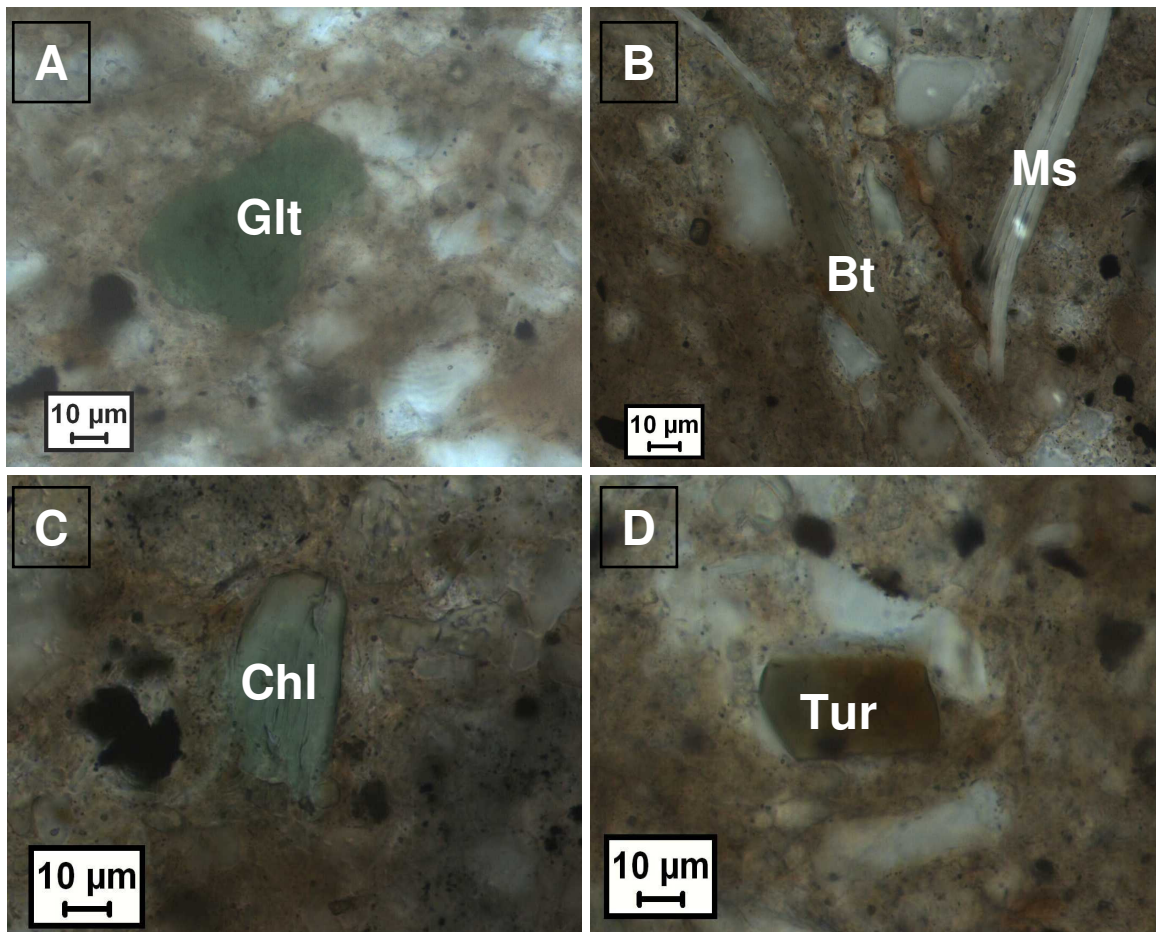


Fig. 1

Figure 1. Optical microscopic observations using transmitted natural light. A, B and D: sample EST 25380; C: sample EST 25687. Glt: glauconite; Bt: biotite; Ms: muscovite; Chl: chlorite; Tur: tourmaline. (*Intended for colour reproduction in print*)

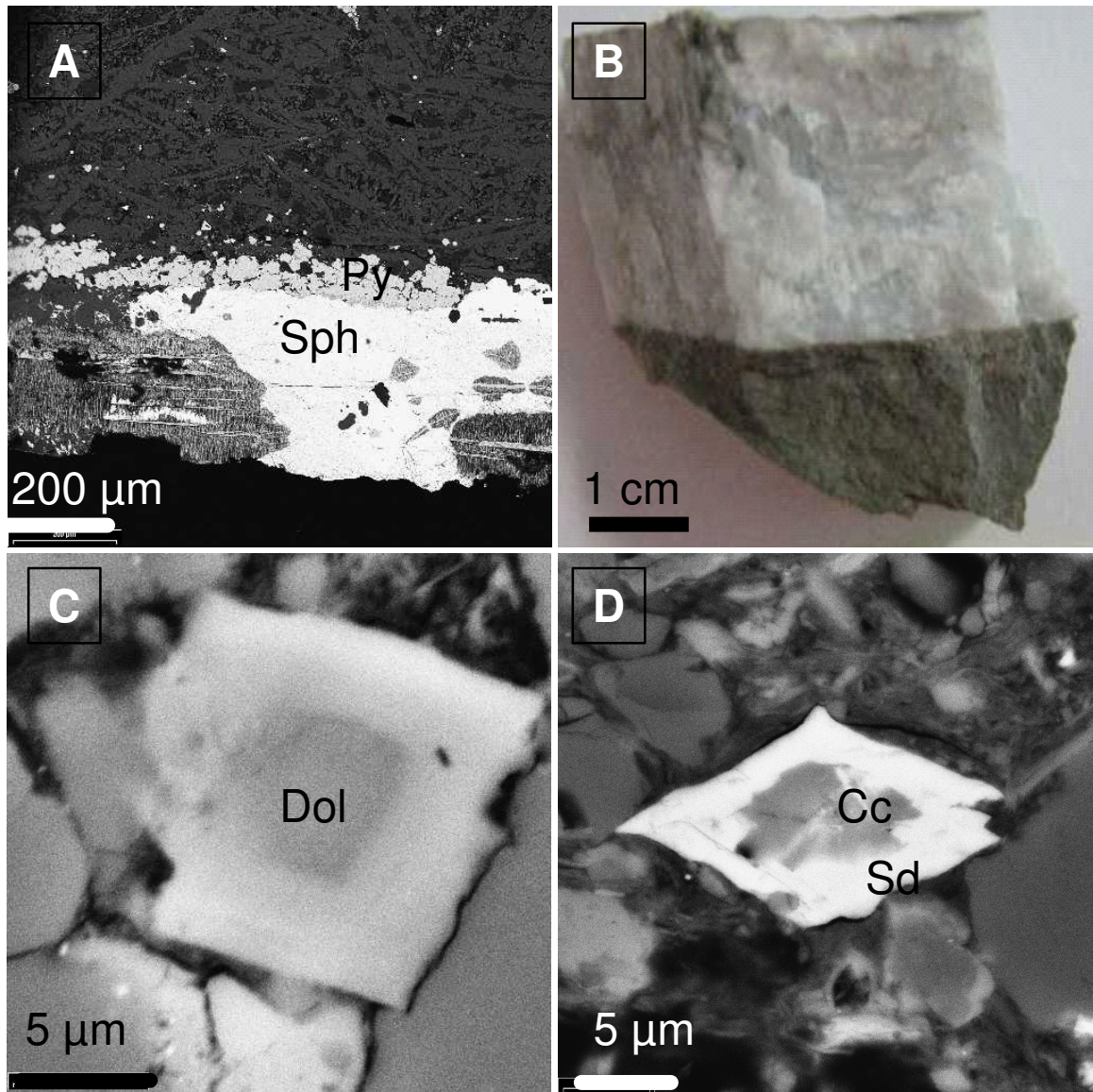


Fig. 2

Figure 2. A: Micrograph of pyrite (Py) and sphalerite (Sph) (backscattered electron image – sample 12436); B: Macrograph of a celestite vein crosscutting the Callovian-Oxfordian formation (Sample EST 20714); Micrograph of an euhedral grain of dolomite with an iron-rich rim (backscattered electron image – sample EST 21400); D: Micrograph of an euhedral grain of carbonate. The core is an iron-rich calcite (Cc), whereas the rim is a siderite (Sd) (backscattered electron image – sample EST 25687). (*Intended for colour reproduction in print*)

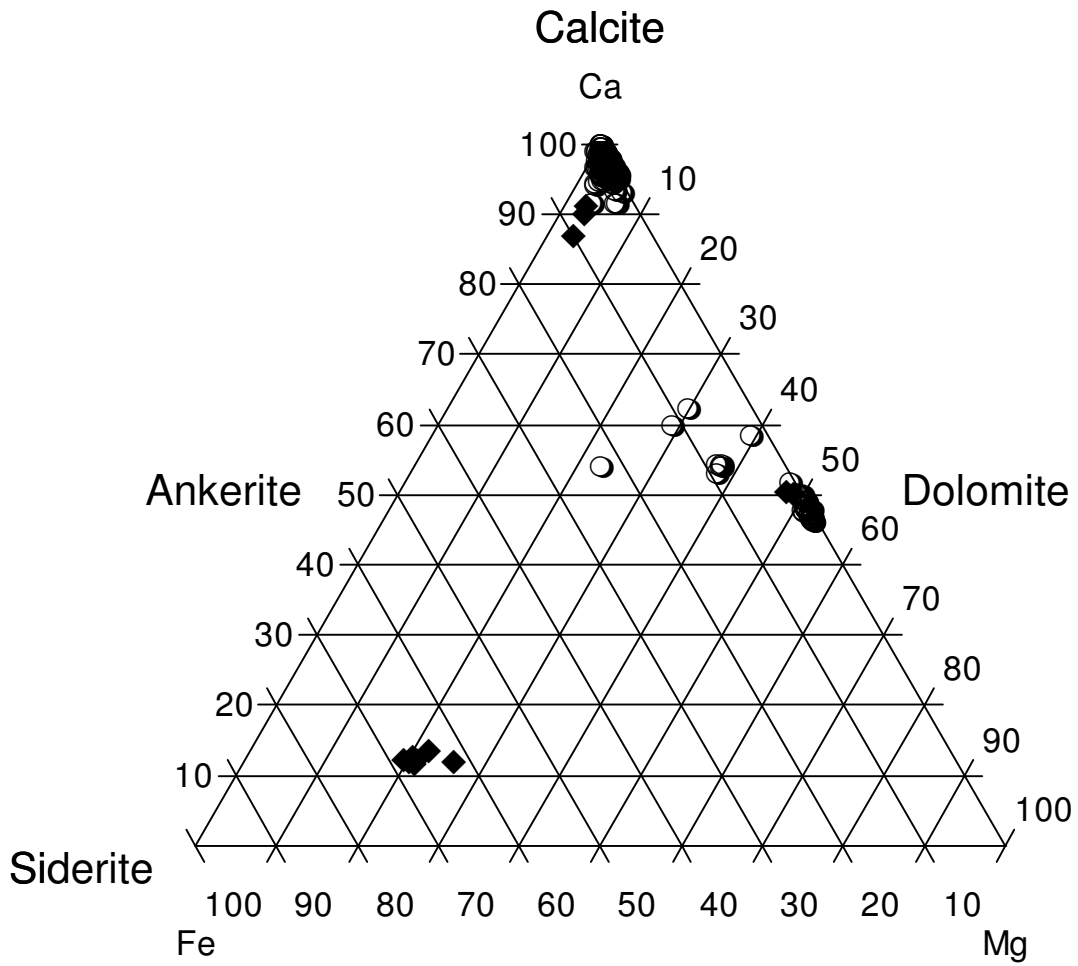


Fig. 3

Figure 3. Triangular Ca-Fe-Mg diagram showing the main chemical compositions of the carbonates in the Callovian-Oxfordian formations. Black symbols correspond to the sample EST 25687 in which siderite grew after iron-rich calcite. Open symbols correspond to all other samples.

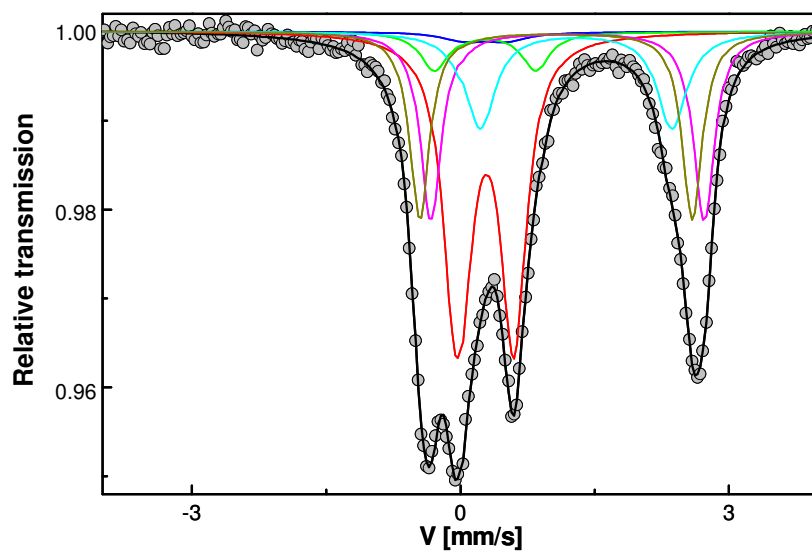


Fig. 4

Figure 4. 77 K Mössbauer spectrum of sample EST 25687. Red, pink, green, light blue and dark blue curves refer to Mössbauer fitting components given in Table 5. The black curve is the sum of all of these contributions. (*Intended for colour reproduction in print*)